Dual-targeting of αvβ3–integrin and galectin-1 improves the specificity of paramagnetic, fluorescent liposome association with tumor endothelium in vivo

E. Kluza[1], I. Jacobs[1], S. J. Hectors[1], K. H. Mayo[2], A. W. Griffioen[3], G. J. Strijkers[1], and K. Nicolay[1]

[1]Biomedical NMR, Department of Biomedical Engineering, Eindhoven University of Technology, Eindhoven, Netherlands, [2]Department of Biochemistry, Molecular Biology and Biophysics, University of Minnesota, Minneapolis, United States, [3]Angiogenesis Laboratory, Department of Medical Oncology, VU Medical Center, Amsterdam, Netherlands

Introduction: Simultaneous targeting of galectin-1 and $\alpha_v\beta_3$-integrin markedly improves the recognition of activated endothelial cells *in vitro* by paramagnetic liposomes as an MRI-detectable nanoparticle [1]. The liposomes were conjugated with peptidic ligands, anginex (Anx) and cyclic RGD (RGD), having a high affinity for galectin-1 and $\alpha_v\beta_3$-integrin, resp. Here, we show that the dual-ligand procedure also enhances molecular MRI of tumor angiogenesis under *in vivo* conditions. Comparisons were made between dual targeted liposomes (Anx/RGD-L) and single targeted liposomes (Anx-L and RGD-L).

Materials and Methods: Liposomes (ø200nm) containing Gd-DTPA-di(stearylamide) and rhodamine-PE for MRI and fluorescence detection, were prepared as in [1]. RGD and anginex were conjugated at 3 and 10μg/μmol lipid. C57BL/6 mice were inoculated *s.c.* with 10^6 B16F10 cells. Studies were done 7-9 days later. Liposomal clearance was determined from T_1 measurements at 6.3T on 20μl blood samples at 9 time points (n=3) between 2min and 48h after injection. *In vivo* MRI was done at 6.3T. Mice (n=6/group) were anaesthetized and liposomes were injected in the tail vein at a dose of 200μmol lipid (50μmol Gd)/kg. MRI scans included: fat-suppressed T_2-w spin-echo (TE/TR=35/4200ms; NA=4); diffusion-weighted spin-echo (TE/TR=35/2000ms; b-value=0 or 400s/mm^2; NA=2). Intratumoral liposome uptake was monitored using T_1-w MRI and T_1 mapping. T_1-w used fat-suppressed spin-echo (TE/TR=8.8/800ms; NA=6), pre- and up to 1.5h post-contrast. T_1 maps were calculated from T_1-w spin-echo images (7 TR from 400-3500ms; TE=8.8ms; NA=1). The latter scans were made pre-, and 2 and 24h post-contrast. For all scans: matrix=128×128; FOV=3×3cm^2; slice=1mm. In addition, two mice injected with Anx/RGD-L or RGD-L were euthanized 2h later to determine the intratumoral liposome distribution at this early time point with fluorescence microscopy. Liposome-induced contrast enhancement on T_1-w images was analyzed pixel-wise. The CNR threshold was set at 5 and the percentage of enhanced pixels in the entire tumor was determined at each time point. T_1s were calculated pixel-wise by fitting the signal intensity to S~1-exp(-TR/T_1). T_1 data were used to assess the R_1 distribution in the entire tumor. R_1 distributions and median values were used for statistical analyses. Microscopy was done on tumors dissected 24h after administration of Anx/RGD-L, Anx-L or RGD-L (n=6 each). 5-μm frozen sections were stained for endothelial cells (CD31) and cell nuclei (DAPI). Images were acquired at 200×magnification, in ≥ 10 regions/tumor. Pixels positive for CD31, rhodamine (liposomes), and both CD31 and rhodamine (indicative of co-localization of liposomes and vascular endothelium) were quantified. Endothelial targeting specificity was expressed as the fraction of rhodamine signal that co-localized with CD31. The fraction of the total endothelial cell area in which rhodamine co-localized with CD31 was used to estimate targeting efficacy. The fraction of the total CD31 positive area was used as an index of tumor vascularity. To determine the liposomal distribution early after injection, the tumors dissected 2h after Anx/RGD-L (n=2) or RGD-L (n=2) injection were analyzed. To assess liposomal bio-distribution, 5 μm sections of liver, spleen, muscle and kidney were stained for macrophages (CD31) and nuclei (DAPI). Data are presented as mean±SD. Median tumor R_1 as well as ΔR_1 and R_1 distributions were compared before, and 2 and 24h after liposome injection.

Results & Discussion: Fig 1 shows the blood clearance kinetics of the three different liposomes. Anx-L and specially Anx/RGD-L were cleared much faster than RGD-L. No liposomes were detectable in blood after 24h. Liposome delivery to tumors was monitored with T_1-w MRI (Fig 2) in the early phase (Fig 3) and with T_1 mapping up to 24h post-injection. Initial signal increases (Fig 3) were very similar for all liposomes. However, the signal changes induced by RGD-L remained largely constant up to 90min, while decreasing for both types of Anx-liposomes. These enhancement pattern differences persisted up to 24h post-contrast, as deduced from pre- and post-contrast R_1 histograms, *i.e.,* RGD-L caused the strongest shift in R_1 distribution and there were no significant differences between Anx/RGD-L and Anx-L. Fluorescence microscopy (Fig 4) was used to obtain semi-quantitative indices of the specificity and efficacy of the liposomal targeting to tumor endothelium (see M&M for definitions) (Fig 5). Anx/RGD-L had the highest specificity of endothelial targeting and the lowest degree of extravasation. RGD-L had the highest targeting efficacy, which we attribute to its longer circulation half-life. In tumors dissected 2h post-injection, Anx/RGD-L were mostly associated with tumor endothelium, similar to that at 24h (Fig 4). RGD-L were mainly in the vessel lumen and a minor proportion was associated with endothelial cells. Tumor vascularity was identical for all groups. Microscopy-based biodistribution data showed that liver and spleen contained high levels of all liposomal systems. No evidence for association to normal endothelium was obtained.

Conclusions: Paramagnetic liposomes that are targeted to two abundant tumor endothelial markers achieve a more specific MRI read-out of tumor angiogenesis than single-ligand particles. These findings will be exploited for diagnostic and therapeutic use.

References: [1] Kluza *et al.* Nano Lett **10**: 52-58, 2010.

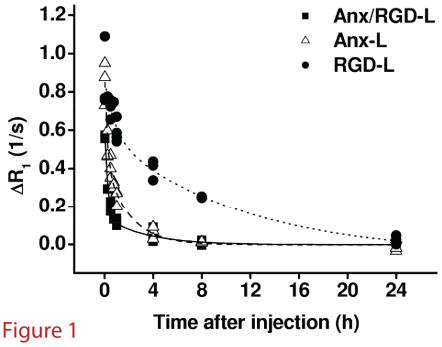

Figure 1

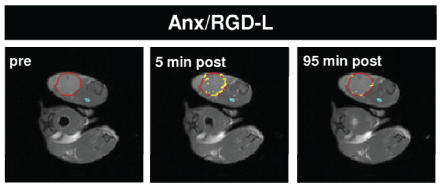

Figure 2

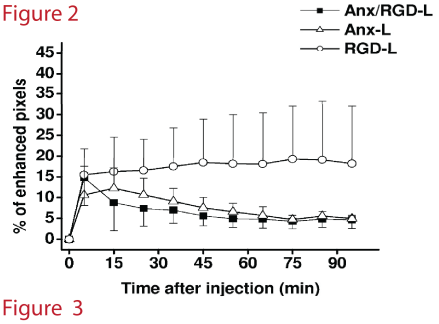

Figure 3

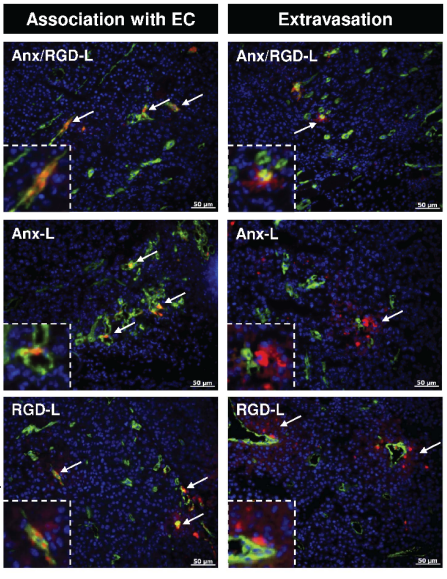

Figure 4

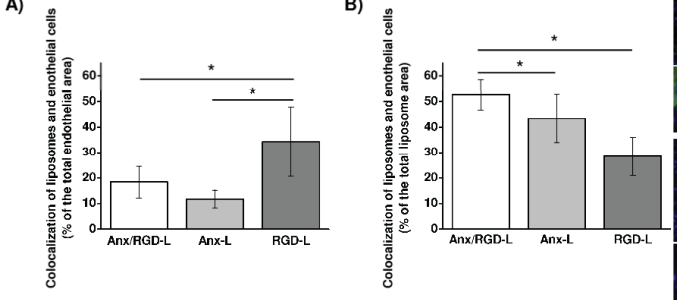

Figure 5